

Kiyoshi Kobayashi · Masateru Nishioka · Koichi Sato ·
Tomoya Inoue · Satoshi Hamakawa · Tatsuo Tsunoda

Synthesis and oxygen permeation properties of 75 mol% $\text{Ce}_{0.75}\text{Nd}_{0.25}\text{O}_{1.875}$ –25 mol% $\text{Nd}_{1.8}\text{Ce}_{0.2}\text{CuO}_4$ composite

Received: 14 December 2005 / Accepted: 25 December 2005 / Published online: 25 April 2006
© Springer-Verlag 2006

Abstract An oxygen-permeable composite constituted to oxide ionic conductor phase ($\text{Ce}_{0.75}\text{Nd}_{0.25}\text{O}_{1.875}$) and oxide electronic conductor phase ($\text{Nd}_{1.8}\text{Ce}_{0.2}\text{CuO}_4$) was prepared using the acetate pyrolysis method. Based on electrical conductivity measurements, total electrical conductivity of 75 mol% $\text{Ce}_{0.75}\text{Nd}_{0.25}\text{O}_{1.875}$ –25 mol% $\text{Nd}_{1.8}\text{Ce}_{0.2}\text{CuO}_4$ composite material was governed by the electronic conduction paths. With respect to the oxygen permeation properties, the results showed that oxygen permeation properties were unexplainable by a simple composite rule using the electrical transport properties of the bulk $\text{Ce}_{0.75}\text{Nd}_{0.25}\text{O}_{1.875}$ and the bulk $\text{Nd}_{1.8}\text{Ce}_{0.2}\text{CuO}_4$.

Keywords Composite · Dual phase · Oxygen permeation · Ceria · Neodymium copper oxide · Acetate pyrolysis · Interface

Introduction

Since Mazanec proposed the materials design concept for the dual-phase oxygen permeable composites [1], oxygen permeation properties of an oxide ionic conductor–noble metal composites and an oxide ionic conductor–oxide

electronic conductor composites have been investigated by numerous researchers [1–23]. Oxygen-permeable composites constituted to an oxide ionic conductor and an oxide electronic conductor have attracted attention because anomalous electrical transport properties or oxygen diffusion and surface reaction have been reported in ($\text{Sc}_2\text{O}_3+\text{Y}_2\text{O}_3$)-doped zirconia– $\text{La}_{0.85}\text{Sr}_{0.15}\text{Mn}_{1.10}\text{O}_\xi$ composite [14] and yttria-stabilized zirconia– $\text{LaSrMnO}_{3-\delta}$ composite [22, 23].

For designing this dual-phase composite constituted to an oxide ionic conductor and an oxide electronic conductor, the electrical transport properties of the constituent phases must be considered. Furthermore, the phase equilibrium must be examined to avoid the chemical reaction and phase decomposition at the interface of an oxide ionic conductor and an electronic conductor because the oxygen-permeable composite membrane is used at high temperatures [19, 20].

For this study, we selected a $\text{Ce}_{0.75}\text{Nd}_{0.25}\text{O}_{1.875}$ – $\text{Nd}_{1.8}\text{Ce}_{0.2}\text{CuO}_4$ system because the combination of these phases is formed as the equilibrium state [24]. It is difficult to fabricate a dense $\text{Ce}_{0.75}\text{Nd}_{0.25}\text{O}_{1.875}$ – $\text{Nd}_{1.8}\text{Ce}_{0.2}\text{CuO}_4$ composite membrane using conventional solid-state reaction method because the reaction and sintering temperature of $\text{Ce}_{0.75}\text{Nd}_{0.25}\text{O}_{1.875}$ (1,923 K) is much higher than the reaction and sintering temperature of $\text{Nd}_{1.8}\text{Ce}_{0.2}\text{CuO}_4$ (1,373 K). However, we succeeded to fabricate the dense composite membrane constituted to 75 mol% $\text{Ce}_{0.75}\text{Nd}_{0.25}\text{O}_{1.875}$ –25 mol% $\text{Nd}_{1.8}\text{Ce}_{0.2}\text{CuO}_4$ employing the acetate pyrolysis method. Using the dense composite, we investigated the oxygen permeation properties of this composite material.

M. Nishioka · K. Sato ·
T. Inoue · S. Hamakawa · T. Tsunoda
National Institute of Advanced Industrial
Science and Technology,
4-2-1, Nigatake,
Miyagino-ku, Sendai 983-8551, Japan

Present address:

K. Kobayashi (✉)
International Center for Young Scientist,
Fuel Cell Materials Center,
National Institute for Materials Science,
1-1, Namiki,
Tsukuba 305-0044, Japan
e-mail: KOBAYASHI.kiyoshi@nims.go.jp
Tel.: +81-29-8604562
Fax: +81-29-8604706

Experimental

Sample preparation

A composite sample with a composition of 75 mol% $\text{Ce}_{0.75}\text{Nd}_{0.25}\text{O}_{1.875}$ –25 mol% $\text{Nd}_{1.8}\text{Ce}_{0.2}\text{CuO}_4$ was prepared using the acetate pyrolysis method. This composition corresponds to 57 vol% $\text{Ce}_{0.75}\text{Nd}_{0.25}\text{O}_{1.875}$ –43 vol% $\text{Nd}_{1.8}\text{Ce}_{0.2}\text{CuO}_4$.

The starting materials were cerium (III) acetate monohydrate, neodymium acetate monohydrate, and copper (II) acetate monohydrate (99.9% purity, Wako, Tokyo, Japan). These raw materials were weighed to the intended composition. Neodymium acetate monohydrate and copper (II) acetate monohydrate were dissolved in distilled water. Then, the cerium (III) acetate monohydrate was added to the solution. The solution became opaque because of the cerium hydroxide dispersion. The solution was heated during stirring on the hot plate to evaporate the water; thereby, we were able to obtain precipitates. The precipitates were heated to about 473 K in a mantle heater for the thermal decomposition.

The residuals were crushed into powder, which was used as the precursor. The precursor was pressed into disks using mechanical pressing at 179 MP; it was heated for 3 h in air at 673, 873, 1,073, 1,273, and 1,323 K. The formation phases were confirmed using X-ray diffraction analyses. Disks with high sintering density were obtained by heating at 1,323 K.

Electrical conductivity

Total electrical conductivity was measured by conventional four-probe DC method between 1,073 and 1,173 K. Oxygen fugacity, p_{O_2} , was changed from $10^{-2.5}$ to 0.21 using the Ar and air mixture. Oxygen fugacity is defined as $p_{O_2} = (P_{O_2}/P^\circ)$ using the oxygen partial pressure (P_{O_2}) and standard pressure (P°). The p_{O_2} values were measured using a zirconia oxygen sensor fixed near the sample.

Oxygen permeation measurements

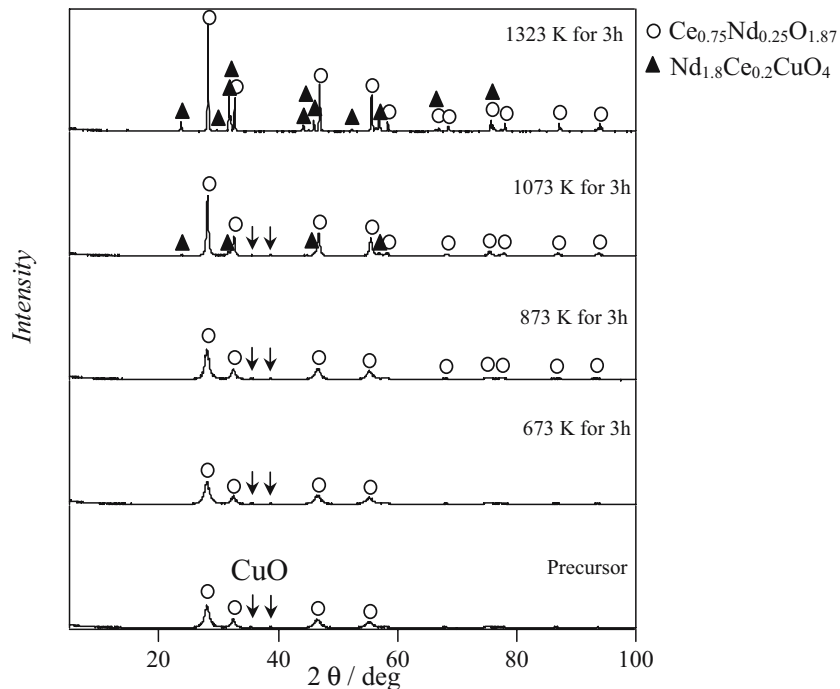
Oxygen permeation flux was measured using the gas flow method with helium and air. Sample thicknesses were 0.58, 0.83, 1.03, 1.81, and 1.13 mm. With respect to the 1.13-mm-thick sample, platinum catalyst was pasted on both of the sample surfaces. In addition, we measured the electromotive force as the oxygen concentration cell using the two platinum wires attached to the platinum catalyst on both of the surfaces of the composite. The sample disks were fixed between two alumina tubes using silver ring seals. The sealing temperature was about 1,223 K. The permeation area was 0.95 cm^2 . After sealing, air flowed at one side of the sample and helium flow at the other side. After reaching the steady state, the electrochemical leakage of oxygen was detected by a gas chromatograph (GC-8A, Shimadzu, Japan). The N_2 concentration at each measurement was measured at that time using gas chromatography. The mechanical leakage was concluded to be negligible because the oxygen permeation rate by the mechanical leakage was estimated as less than 1% of oxygen permeation rate by the electrochemical leakage through the sample. The p_{O_2} at the surface of oxygen-permeated side $p_{O_2}^{\text{perm}}$ was changed by changing the helium gas flow rate of between 100 and 5 ml/min. The $p_{O_2}^{\text{perm}}$ values were assumed as equivalent to the oxygen fugacity of the outlet gas.

Results

Characterization by X-ray diffraction analyses

The X-ray diffraction profiles of the precursor and samples heated for 3 h in air at 673, 873, 1,073, and 1,323 K are

Fig. 1 X-ray powder diffraction profiles of 75 mol% $Ce_{0.75}Nd_{0.25}O_{1.875}$ –25 mol% $Nd_{1.8}Ce_{0.2}CuO_4$ powder heat-treated at 623 (precursor), 873, 1,073, and 1,323 K for 3 h in air. Identified peaks are labeled as: CeO_2 with fluorite structure (open circle) and Nd_2CuO_4 with K_2NiF_4 structure (closed triangle). Small peaks of CuO are shown by arrows



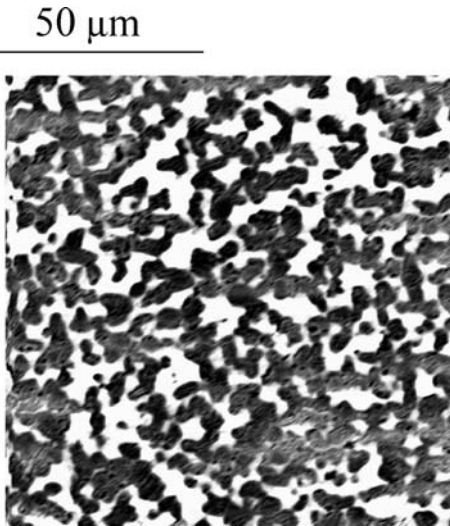


Fig. 2 Microstructure of 75 mol% $\text{Ce}_{0.75}\text{Nd}_{0.25}\text{O}_{1.875}$ –25 mol% $\text{Nd}_{1.8}\text{Ce}_{0.2}\text{CuO}_4$ composite sintered at 1,323 K. The lighter part is an oxide ionic conduction phase ($\text{Ce}_{0.75}\text{Nd}_{0.25}\text{O}_{1.875}$); the darker part is an electronic conduction phase ($\text{Nd}_{1.8}\text{Ce}_{0.2}\text{CuO}_4$)

shown in Fig. 1. The profiles of the sample that was heat-treated below 873 K mainly comprised peaks that were assignable to the CeO_2 phase with fluorite structure. We were able to find the small peaks of CuO phase. On the other hand, the small peaks assigned to Nd_2CuO_4 phase appeared by heating at 1,073 K; the peaks of Nd_2CuO_4 phase grew and CuO peaks disappeared by heating at 1,323 K.

The microstructure of the 75 mol% $\text{Ce}_{0.75}\text{Nd}_{0.25}\text{O}_{1.875}$ –25 mol% $\text{Nd}_{1.8}\text{Ce}_{0.2}\text{CuO}_4$ heat-treated at 1,323 K for 3 h in air is shown in Fig. 2. The particles of the electronic conduction phase ($\text{Nd}_{1.8}\text{Ce}_{0.2}\text{CuO}_4$) are about 20–30 μm .

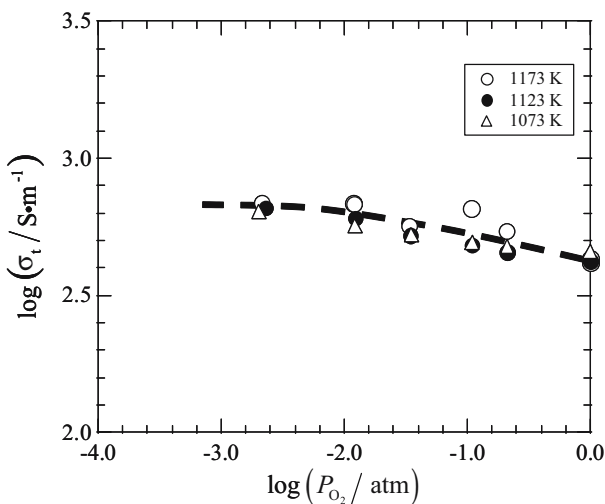


Fig. 3 Relationship between total electrical conductivity and logarithm of the oxygen fugacity for the 75 mol% $\text{Ce}_{0.75}\text{Nd}_{0.25}\text{O}_{1.875}$ –25 mol% $\text{Nd}_{1.8}\text{Ce}_{0.2}\text{CuO}_4$ composite

Electrical conductivity and oxygen permeability

Total electrical conductivity (σ_t) was revealed as almost independent of p_{O_2} with a temperature, which is similar to the electrical transport properties of CeO_2 -doped Nd_2CuO_4 [25, 26], as shown in Fig. 3. Moreover, we confirmed that the electromotive force was equal to 0 during oxygen permeation when the composite was used as the electrolyte for the oxygen concentration cell. Hence, the σ_t of 75 mol% $\text{Ce}_{0.75}\text{Nd}_{0.25}\text{O}_{1.875}$ –25 mol% $\text{Nd}_{1.8}\text{Ce}_{0.2}\text{CuO}_4$ is governed by the electronic conduction paths generated by the $\text{Nd}_{1.8}\text{Ce}_{0.2}\text{CuO}_4$ connections.

Although a plot of the oxygen permeation flux J_{O_2} vs $\log(p_{\text{O}_2}^{\text{feed}}/p_{\text{O}_2}^{\text{perm}})$ showed a linear relationship, the lines

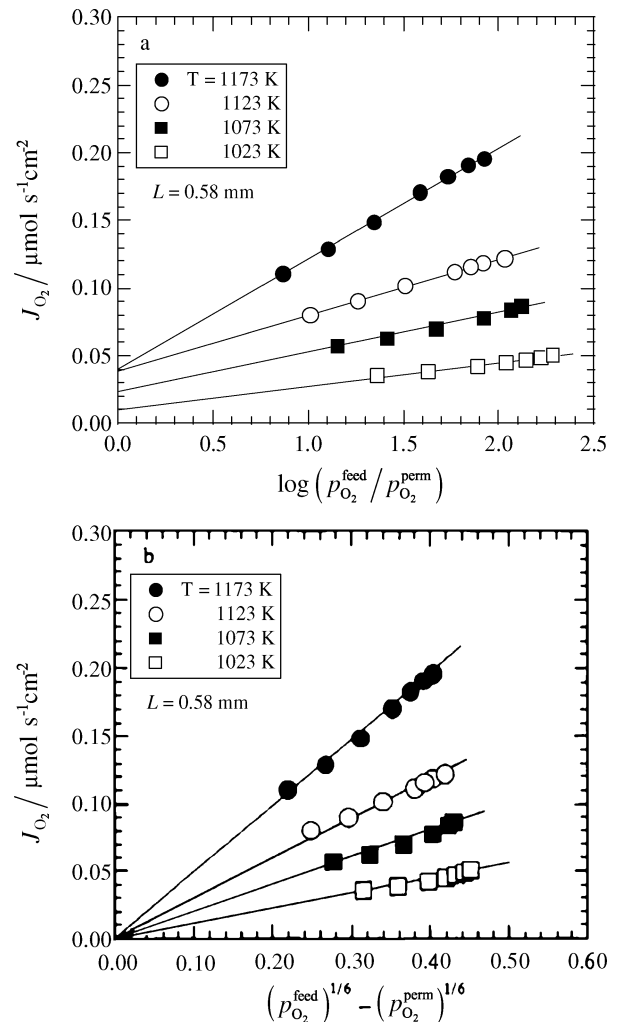


Fig. 4 Dependences of oxygen fugacity difference on oxygen permeation flux (J_{O_2}) for 75 mol% $\text{Ce}_{0.75}\text{Nd}_{0.25}\text{O}_{1.875}$ –25 mol% $\text{Nd}_{1.8}\text{Ce}_{0.2}\text{CuO}_4$ composite: **a** Relationship between J_{O_2} and logarithm of the oxygen fugacity difference between the oxygen feed side and oxygen permeated side ($\log(p_{\text{O}_2}^{\text{feed}}/p_{\text{O}_2}^{\text{perm}})$). **b** Relationship between J_{O_2} and difference of one sixth power of oxygen fugacity ($(p_{\text{O}_2}^{\text{feed}})^{1/6} - (p_{\text{O}_2}^{\text{perm}})^{1/6}$)

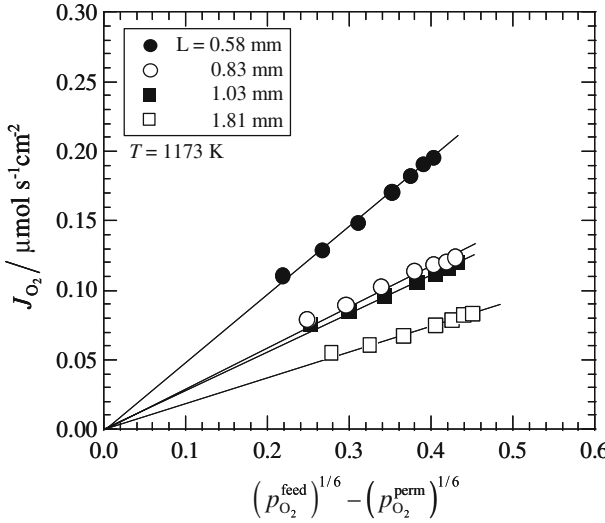


Fig. 5 Variations of the oxygen permeation flux (J_{O_2}) with $(p_{O_2}^{\text{feed}})^{1/6} - (p_{O_2}^{\text{perm}})^{1/6}$ for 75 mol% $\text{Ce}_{0.75}\text{Nd}_{0.25}\text{O}_{1.875}$ –25 mol% $\text{Nd}_{1.8}\text{Ce}_{0.2}\text{CuO}_4$ composite samples with the different thickness of 0.58, 0.83, 1.03, and 1.81 mm at 1,173 K

did not intersect with the origin, as shown in Fig. 4a. The relationship between the J_{O_2} and $(p_{O_2}^{\text{feed}})^{1/6} - (p_{O_2}^{\text{perm}})^{1/6}$ was linear through the origin (Fig. 4b). The J_{O_2} values increased with decreasing sample thickness (Fig. 5). The relationship between the J_{O_2} at $p_{O_2}^{\text{feed}}/p_{O_2}^{\text{perm}} = 10$ ($J_{O_2}^*$) and reciprocal sample thickness (L^{-1}) is scattered slightly, but the plot showed a linear relationship across the origin (Fig. 6).

Only a small influence of J_{O_2} on the addition to the platinum catalyst on both surfaces appeared, as shown

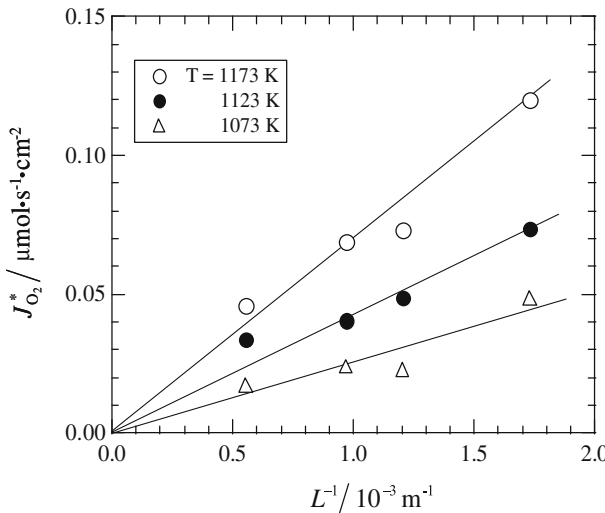


Fig. 6 Relationship between the oxygen permeation flux at $p_{O_2}^{\text{feed}}/p_{O_2}^{\text{perm}} = 10$ ($J_{O_2}^*$) and reciprocal sample thickness for 75 mol% $\text{Ce}_{0.75}\text{Nd}_{0.25}\text{O}_{1.875}$ –25 mol% $\text{Nd}_{1.8}\text{Ce}_{0.2}\text{CuO}_4$ composites at 1,173, 1,123, and 1,073 K

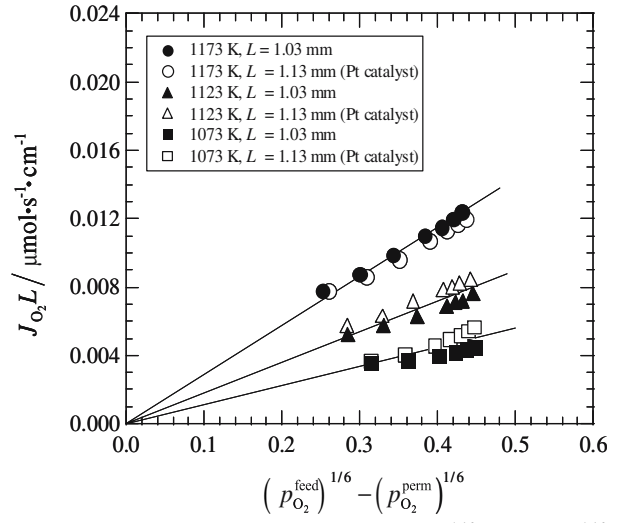


Fig. 7 Relationships between $J_{O_2}L$ and $(p_{O_2}^{\text{feed}})^{1/6} - (p_{O_2}^{\text{perm}})^{1/6}$ of the 75 mol% $\text{Ce}_{0.75}\text{Nd}_{0.25}\text{O}_{1.875}$ –25 mol% $\text{Nd}_{1.8}\text{Ce}_{0.2}\text{CuO}_4$ composite with platinum catalyst on both of the sample surfaces and the composite without the catalyst

in Fig. 7. If the oxygen permeation flux is limited by the surface reaction rate as a result of the insufficient triple-phase boundary area among an oxide ionic conduction phase ($\text{Ce}_{0.75}\text{Nd}_{0.25}\text{O}_{1.875}$), an oxide electronic conduction phase ($\text{Nd}_{1.8}\text{Ce}_{0.2}\text{CuO}_4$), and gas phase at the surface, then a drastic increase of the J_{O_2} might occur by pasting the platinum catalyst because of increasing the triple-phase boundary area on the surface. Considering the dependence of the sample thickness on the J_{O_2} , along with the influence of the catalyst addition on the J_{O_2} , as shown in Figs. 4, 5, 6 and 7, it is suggested that the main limiting process of the oxygen permeation is the conduction of the oxide ions in the composite.

Discussion

It is assumed that the oxide ions and electrons are conducted, respectively, in the oxide ionic conduction paths and in the electronic conduction paths during the oxygen permeation. The oxygen flux (J_{O_2}) and electronic flux $J_{e'}$ are given as [27, 28]

$$J_{O_2} = -\frac{\sigma_{O^{2-}}^{\text{CNO}}}{4F^2} \frac{\partial \eta_{O^{2-}}^{\text{CNO}}}{\partial x}, \quad (1)$$

and

$$J_{e'} = -\frac{\sigma_{e'}^{\text{NCCO}}}{F^2} \frac{\partial \eta_{e'}^{\text{NCCO}}}{\partial x}, \quad (2)$$

where $\sigma_{O^{2-}}^{\text{CNO}}$ and $\sigma_{e'}^{\text{NCCO}}$ are the effective oxide ionic conductivity of $\text{Ce}_{0.75}\text{Nd}_{0.25}\text{O}_{1.875}$ paths and the effective electronic conductivity of $\text{Nd}_{1.8}\text{Ce}_{0.2}\text{CuO}_4$ paths. The

$\eta_{O^{2-}}^{\text{CNO}}$ is the electrochemical potential of oxide ions in $\text{Ce}_{0.75}\text{Nd}_{0.25}\text{O}_{1.875}$ paths and $\eta_{e'}^{\text{NCCO}}$ is the electrochemical potential of electrons in $\text{Nd}_{1.8}\text{Ce}_{0.2}\text{CuO}_4$ paths. If the equilibrium condition of the electrochemical potentials is established at the $\text{Ce}_{0.75}\text{Nd}_{0.25}\text{O}_{1.875}/\text{Nd}_{1.8}\text{Ce}_{0.2}\text{CuO}_4$ hetero-junction in the composite, then the following relationships pertain:

$$\eta_{O^{2-}}^{\text{CNO}} = \eta_{O^{2-}}^{\text{NCCO}} \text{ and } \eta_{e'}^{\text{CNO}} = \eta_{e'}^{\text{NCCO}}. \quad (3)$$

Therein, $\eta_{O^{2-}}^{\text{NCCO}}$ and $\eta_{e'}^{\text{CNO}}$ are the electrochemical potential of oxide ions in $\text{Nd}_{1.8}\text{Ce}_{0.2}\text{CuO}_4$ and the potential of electrons in $\text{Ce}_{0.75}\text{Nd}_{0.25}\text{O}_{1.875}$. In addition, the equilibrium condition of neutral oxygen (O) in $\text{Ce}_{0.75}\text{Nd}_{0.25}\text{O}_{1.875}$ and $\text{Nd}_{1.8}\text{Ce}_{0.2}\text{CuO}_4$ are given using the chemical potential of $\text{O}_2(\mu_{O_2})$ as

$$\mu_O^{\text{CNO}} = \mu_O^{\text{NCCO}} = \frac{1}{2}\mu_{O_2} = \frac{1}{2}(\mu_{O_2}^o + RT \ln p_{O_2}), \quad (4)$$

where μ_O^{CNO} and μ_O^{NCCO} are the chemical potentials of O in $\text{Ce}_{0.75}\text{Nd}_{0.25}\text{O}_{1.875}$ and $\text{Nd}_{1.8}\text{Ce}_{0.2}\text{CuO}_4$, respectively, and $\mu_{O_2}^o$ is the standard chemical potential of O_2 . In addition, the electrical neutrality of the oxide ionic flux and electronic flux during the oxygen permeation must be established as

$$4J_{O_2} = J_{e'}. \quad (5)$$

Hence, the oxygen permeation flux can be led to combinations of Eqs. 1, 2, 3, 4 and 5:

$$J_{O_2} = -\frac{RT}{16F^2L} \int_{\ln p_{O_2}^{\text{feed}}}^{\ln p_{O_2}^{\text{perm}}} \frac{\sigma_{O^{2-}}^{\text{CNO}} \sigma_{e'}^{\text{NCCO}}}{\sigma_{O^{2-}}^{\text{CNO}} + \sigma_{e'}^{\text{NCCO}}} d \ln p_{O_2}. \quad (6)$$

In that equation, L is the distance between the oxygen-fed side and oxygen-permeated side of the sample. Based on the σ_t measurements, as shown in Fig. 3, and electromotive force measurements, the $\sigma_{e'}^{\text{NCCO}}$ values are much larger than the $\sigma_{O^{2-}}^{\text{CNO}}$ values, and Eq. 6 can be rewritten as

$$J_{O_2} = -\frac{RT}{16F^2L} \int_{\ln p_{O_2}^{\text{feed}}}^{\ln p_{O_2}^{\text{perm}}} \sigma_{O^{2-}}^{\text{CNO}} d \ln p_{O_2}. \quad (7)$$

If the $\sigma_{O^{2-}}^{\text{CNO}}$ values are independent of p_{O_2} in this experimental region as the same with the oxide ionic conductivity of bulk $\text{Ce}_{0.75}\text{Nd}_{0.25}\text{O}_{1.875}$, the plot of J_{O_2} vs $\log(p_{O_2}^{\text{feed}}/p_{O_2}^{\text{perm}})$ must show a linear relationship through the origin from Eq. 7. However, the experimental results did not support that expectation. In contrast to the bases of the experimental results, the $\Delta p_{O_2}^{1/6}$ depended on

J_{O_2} as shown in Fig. 4b, meaning that $\sigma_{O^{2-}}^{\text{CNO}}$ is proportional to $p_{O_2}^{1/6}$ from the Eq. 7.

Establishing to the local equilibrium at the $\text{Ce}_{0.75}\text{Nd}_{0.25}\text{O}_{1.875}/\text{Nd}_{1.8}\text{Ce}_{0.2}\text{CuO}_4$ hetero-junction interface (Eqs. 3 and 4), the concentrations of the constituent elements, including the oxide ion vacancy, close to the hetero-junction should differ from the concentrations in the bulk that are created by the formation of the space charge layer [29–32]. The oxygen permeation properties of the $\text{Ce}_{0.75}\text{Nd}_{0.25}\text{O}_{1.875}-\text{Nd}_{1.8}\text{Ce}_{0.2}\text{CuO}_4$ composite were unexplainable using the simple composite rule with the electrical transport properties of the $\text{Ce}_{0.75}\text{Nd}_{0.25}\text{O}_{1.875}$ phase and $\text{Nd}_{1.8}\text{Ce}_{0.2}\text{CuO}_4$ phase if the oxide ionic conduction properties for the oxygen permeation were strongly influenced by conduction properties of the space charge layer.

With respect to the anomalous electrical conductivity of the composite material constituted to an oxide ionic conductor and an oxide electronic conductor, Bonanos et al. have reported that abnormal oxide ionic conductivity appeared for the $(\text{Sc}_2\text{O}_3+\text{Y}_2\text{O}_3)$ -stabilized zirconia and $\text{La}_{0.85}\text{Sr}_{0.15}\text{Mn}_{1.10}\text{O}_\xi$ composite, with the composition close to the percolation threshold [14]. We have also confirmed the anomalous AC conductivity dispersion in the high-frequency region for $\text{Ce}_{0.75}\text{Nd}_{0.25}\text{O}_{1.875}-\text{Nd}_{1.8}\text{Ce}_{0.2}\text{CuO}_4$ composite with the composition close to the percolation threshold of $\text{Nd}_{1.8}\text{Ce}_{0.2}\text{CuO}_4$ phase (Kobayashi et al., prepared for publish). Based on these results, the space charge layer with specific conduction properties is suggested to exist close to the oxide ionic conductor/oxide electronic conductor junction in the composite material. However, we were unable to explain the physical meaning of the p_{O_2} dependences for J_{O_2} as shown in Fig. 4b. Therefore, further study is necessary to clarify the oxygen permeation properties and electrical transport properties of the region close to the $\text{Ce}_{0.75}\text{Nd}_{0.25}\text{O}_{1.875}/\text{Nd}_{1.8}\text{Ce}_{0.2}\text{CuO}_4$ junction in the composite.

Conclusions

A dense composite membrane with the composition of 75 mol% $\text{Ce}_{0.75}\text{Nd}_{0.25}\text{O}_{1.875}$ –25 mol% $\text{Nd}_{1.8}\text{Ce}_{0.2}\text{CuO}_4$ was synthesized by heat treatment at 1,323 K using the precursor prepared through the acetate pyrolysis route. Based on the conductivity measurements, the total electrical conductivity was governed by the electronic conduction phase ($\text{Nd}_{1.8}\text{Ce}_{0.2}\text{CuO}_4$). It was found that the oxygen fugacity dependence of the oxygen permeation flux was not explained by the simple composite rule using the electrical transport properties of bulk $\text{Ce}_{0.75}\text{Nd}_{0.25}\text{O}_{1.875}$ and bulk $\text{Nd}_{1.8}\text{Ce}_{0.2}\text{CuO}_4$. Based on our results, it is speculated that the specific electrical conduction properties exist close to the $\text{Ce}_{0.75}\text{Nd}_{0.25}\text{O}_{1.875}/\text{Nd}_{1.8}\text{Ce}_{0.2}\text{CuO}_4$ hetero-junction in the composite.

References

1. Mazanec TJ, Cable TL, Frye JG Jr (1992) Solid State Ionics 53–56:111
2. Kruidhof H, Bouwmeester HJM, van Doorn RHE, Burggraaf AJ (1993) Solid State Ionics 63–65:816
3. Chen CS, Boukamp BA, Bouwmeester HJM, Cao GZ, Kruidhof H, Winnubst AJA, Burggraaf AJ (1995) Solid State Ionics 76:23
4. Chen S, Boukamp BA, Bouwmeester HJM, Verweij H, Burggraaf AJ (1996) Solid State Ionics 86–88:569
5. Chen CS, Kruihof H, Bouwmeester HJM, Verweij H, Brugggraaf AJ (1997) Solid State Ionics 99:215
6. ten Elshof JE, Nguyen NQ, den Otter MW, Bouwmeester HJM (1997) J Electrochem Soc 144:4361
7. Huang K, Schroeder M, Goodenough JB (1999) Electrochem Solid-state Lett 2:375
8. Chen CS, Brugggraaf AJ (1999) J Appl Electrochem 29:355
9. Lee TH, Yang YL, Jacobson AJ (2000) Solid State Ionics 134:331
10. Wu K, Xie S, Jiang GS, Liu W, Chen CS (2001) J Membr Sci 188:189
11. Kobayashi K, Tsunoda T (2002) Oxygen permeability of 60-volume% $\text{Bi}_{1.6}\text{Y}_{0.4}\text{O}_3$ and 40-volume% Ag composite prepared by citrate sol–gel method. In: Chowdari BVR, Prabaharan SRS, Yahaya M, Talib IA (eds) Solid state ionics: trends in new millennium. World Scientific, pp 537–544
12. Kobayashi K, Tsunoda T (2004) Solid State Ionics 175:405
13. Esquirol A, Kilner J, Brandon N (2004) Solid State Ionics 175:63
14. Bonanos N, Steele BCH, Butler EP (2005) Application of impedance spectroscopy: characterization of materials. In: Barsoukov E, Macdonald JR (eds) Impedance spectroscopy, theory, experiment, and applications. Wiley-Interscience, New Jersey, pp 205–264
15. Römer EWJ, Nigge U, Schulte T, Wiemhöfer H-D, Bouwmeester HJM (2001) Solid State Ionics 140:97
16. Costa ADS, Labrincha JA, Marques FMB (1995) Solid State Ionics 81:85
17. Kharton VV, Kovalevsky AV, Viskup AP, Figueiredo FM, Yaremchenko AA, Naumovich EN, Marques FMB (2000) J Electrochem Soc 147:2814
18. Kharton VV, Kovalevsky AV, Viskup AP, Figueiredo FM, Yaremchenko AA, Naumovich EN, Marques FMB (2001) J Eur Ceram Soc 21:1763
19. Kharton VV, Kovalevsky AV, Viskup AP, Shaula AL, Figueiredo FM, Naumovich EN, Marques FMB (2003) Solid State Ionics 160:247
20. Shaula AL, Kharton VV, Marques FMB, Kovalevsky AV, Viskup AP, Naumovich EN (2004) Br Ceram Trans 103:211
21. Nigge U, Wiemhöfer H-D, Römer EWJ, Bouwmeester HJM, Schulte TR (2002) Solid State Ionics 146:163
22. Ji Y, Kilner JA, Carolan MF (2005) Solid State Ionics 176:937
23. Ji Y, Kilner JA, Carolan MF (2004) J Eur Ceram Soc 24:3613
24. Huang TC, Moran E, Nazzal AI, Torrance JB (1989) Physica C 158:148
25. Spinolo G, Scavini M, Ghigna P, Chiodelli G, Flor G (1995) Physica C 254:359
26. Yamaguchi S, Yasui K, Matsumoto F, Terabe K, Sukigara T, Iguchi Y (1991) Solid State Ionics 49:63
27. Wagner C (1957) Proceedings of the International Committee of Electrochemical Thermodynamics and Kinetics 7:361
28. Kudo T, Fueki K (1990) Electric conduction in mixed conductors. In: Solid state ionics. Kodansha, Japan, pp 47–63
29. Wagner C (1972) J Phys Chem Solids 33:1051
30. Maier J (1987) J Electrochem Soc 134:1524
31. Maier J (1989) Ber Bunsenges Phys Chem 93:1468
32. Bredikhin S, Hattori T, Ishigame M (1994) Phys Rev B 50:2444